Korean J. Chem. Eng., 37(12), 2192-2201 (2020)
DOI: 10.1007/s11814-020-0629-8

pISSN: 0256-1115
eISSN: 1975-7220

Adsorption of Direct Red 23 dye from aqueous solution by means of modified montmorillonite nanoclay as a superadsorbent: Mechanism, kinetic and isotherm studies

Seyedeh Mahtab Pormazar*, and Arash Dalvand*,†**

*Environmental Science and Technology Research Center, Department of Environmental Health Engineering, School of Public Health, Shahid Sadoughi University of Medical Sciences, Yazd, Iran
**Student Research Committee, Shahid Sadoughi University of Medical Sciences, Yazd, Iran
(*Received 18 April 2020 • Revised 30 June 2020 • Accepted 7 July 2020*)

Abstract−A novel adsorbent of modified nanoclay was synthesized by covering of alum on the montmorillonite nanoclay (Al/nanoclay). Al/nanoclay was applied as an efficient superadsorbent to remove Direct Red 23 (DR23) from colored wastewater. The adsorbent was characterized by Fourier transform infrared spectroscopy, energy-dispersive X-ray spectroscopy, and zeta potential analysis. The effects of various operating parameters, such as contact time, initial dye concentration, adsorbent dose, pH and ionic strength on the performance of adsorption, have been studied. The adsorption experiments showed that pH has an obvious effect on the adsorption efficiency and the highest percentage of DR23 dye removal was observed at pH 2. Zeta potential measurement confirmed that the adsorption mechanism is ascribed to electrostatic interaction between sulfonic groups of the anionic dye and the positive surface charge of the adsorbent. The pseudo-second-order kinetic model and the Langmuir isotherm were found to best describe the DR23 adsorption and the maximum monolayer adsorption capacity at the conditions of pH 2 and the adsorbent dose of 0.05 g/L was 2,500 mg/g. The findings recommend that Al/nanoclay can be successfully used for DR23 dye removal from the colored wastewater.

Keywords: Adsorption, Direct Red 23 Dye, Mechanism, Modified Montmorillonite Nanoclay

INTRODUCTION

Pollution of surface and groundwater resources by synthetic dyes is a severe environmental concern for human health and the ecosystem [1]. Many industries, such as textiles, cosmetics, plastic, and paper are widely using dyes in their processes. Researches indicate that approximately 10-15% of synthetic dyes used annually across the globe are lost during processing operations [2]. Azo dyes are one of the largest and most important classes of synthetic dyes containing naphthalene and/or benzene aromatic rings [3]. Effluents containing azo dyes are dangerous due to their toxicity and carcinogenicity, so elimination of them from the effluent stream is essential [4]. However, it is difficult to remove these dyes due to their complex aromatic structures [5]. There are many technologies to treat textile wastewater such as biological processes [6], coagulation and flocculation [7], electrochemical [8], membrane filtration [9], ozonation [10], advanced oxidation [11] and adsorption processes [12]. Due to the low rates of biodegradability of dyes, biological treatment alone is not very effective [13]. Also, other mentioned techniques have certain disadvantages, including high cost, high sludge production, high energy demand, technical constraints, and the formation of hazardous byproducts [14]. The adsorption process has been considered as an efficient and inexpensive choice for dye removal from wastewater [15]. Different adsorbents like activated carbon [16], zeolites [17], fly ash [18], and other porous materials have been prepared and used in the adsorption of dye. Clay minerals and their derivatives have also been widely used as adsorbent due to their cost-effectiveness, natural abundance, non-toxicity and environmental friendliness [19].

Montmorillonite is a type of natural clay mineral with the chemical formula of $(Na, Ca)_{0.33}(Al, Mg)_2(Si_4O_{10})(OH)_2\ XH_2O$ [20]. It is classified as 2 : 1 clay which consists of alumina (Al^{3+}) octahedral sheet sandwiched between two silica (Si^{4+}) tetrahedral sheets [21]. However, the layers of montmorillonite carry a permanent negative charge due to isomorphous substitution of Al^{3+}, Si^{4+}, Mg^{2+}, and Fe^{3+} ions. Some other 2 : 1 clay minerals (less than 1%) have a positive charge that is caused by broken bonds along particle edges and pH-dependence [22-24]. So, pristine montmorillonite is unsuitable for removing anionic pollutants from aqueous solutions. The changes in the molecular structure and properties of these compounds could lead to significant differences in the clay efficiency, which are suitable for removing organic pollutants [25].

Different chemical components have been used for surface modification of nanoclay to eliminate various types of dyes from wastewater. Dimethyl dialkyl amine [26], dodecyl trimethylammonium bromide [19], and octadecylamine [27] are some of the materials utilized for modification of nanoclay.

Direct Red 23 (DR23) azo dye is an anionic dye widely used for dyeing in several industries, especially the textile industry [28]. In the present study, alum was used to modify the nanoclay mineral

†To whom correspondence should be addressed.
E-mail: arash.dalvand@gmail.com

surface properties. It has been used as a high capacity adsorbent for removing DR23 anionic dye. The effect of some different operational parameters, such as contact time, adsorbent dose, initial adsorbate concentration, pH, and ionic strength on the removal efficiency and adsorption capacity of DR23 was investigated.

MATERIALS AND METHODS

1. Materials

DR23 with $C_{35}H_{25}N_7Na_2O_{10}S_2$ chemical formula and molecular weight of 813.7 g/mol was purchased from Ciba Company. Different concentrations of DR23 were obtained from a stock of 1,000 mg/L dye solution. The montmorillonite nanoclay was provided by Nanosav Company, Iran. All the other chemicals used in this study, including HCL, NaOH, NaCl, and alum ($Al_2(SO_4)_3 \cdot 18H_2O$), were supplied from Merck (Germany). According to the supplier datasheet, the montmorillonite interlayer space was about 5 nm and its density value was 0.6 g/cm^3.

2. Modification of Montmorillonite Nanoclay

To modify nanoclay, 1.5 g nanoclay and 0.375 g alum were poured into 10 mL distilled water and mixed at room temperature for 1 hour. The resulting product was placed in the oven for 1 hour at 120 °C to dry. Then it was put in the furnace for 2 hours at 420 °C. The modified nanoclay powder was kept in the desiccator for later use.

3. Adsorption Experiments

Adsorption equilibrium experiments were conducted by adding different amounts of Al/nanoclay (0.05-0.4 g/L) into an Erlenmeyer flask containing 50 mL of synthetic wastewater with desired DR23 dye concentration (25-200 mg/L). The solution pH was adjusted by adding 0.1 M HCl or NaOH in the range of 2-10. The samples were shaken at the constant agitation speed of 250 rpm at different time intervals (2-90 min). An incubator shaker (Innova40, Germany) was used to control the temperature at 25 °C. After the adsorption process, the samples were taken from the shaker at a predetermined time and filtered through a 0.45 μm filter. The concentration of DR23 dye was determined by UV-Visible spectrometer (HACH, DR6000, USA) at a wavelength of 505 nm. The concentration of the DR23 before and after the adsorption process was used to calculate the amount of dye adsorption. The percentage removal of dye (%) and adsorption capacity (q) were calculated using the following equations:

$$\text{Dye removal efficiency}\ (\%) = \frac{C_0 - C}{C_0} \times 100 \quad (1)$$

$$\text{Adsorption capacity}\ (\text{mg/g}) = \frac{C_0 - C_e}{M} V \quad (2)$$

where C_0 (mg/L) is the initial dye concentration, C is the dye concentration at time t (min) [29], C_e (mg/L) is the equilibrium concentration of dye remaining in the solution, V (L) is the volume of the aqueous solution and M (g) is the mass of Al/nanoclay [30,31].

4. Characterization of the Adsorbent

Zeta potential of modified nanoclay and DR23 dye solution was measured by using a zeta potential analyzer (Malvern, ZEN 3600, UK). The composition of the modified nanoclay was determined by energy dispersive X-ray spectroscopy (EDX). Fourier-transform infrared (FTIR) spectroscopy (Spectrum Two, Perkin Elmer Co, USA) was used to obtain the infrared spectrum of Al/nanoclay.

RESULTS AND DISCUSSION

1. Characterization of Al/Nanoclay

The FTIR spectrum of modified nanoclay was recorded in the wavenumber range between 400 and 4,000 cm^{-1}. The infrared spectrum of Al/nanoclay is shown in Fig. 1. The presence of the strong peak at 1,044 cm^{-1} was assigned to Si-O stretching vibrations. Also, the peaks at 797 cm^{-1} and 916 cm^{-1} could be attributed to Si-O stretching

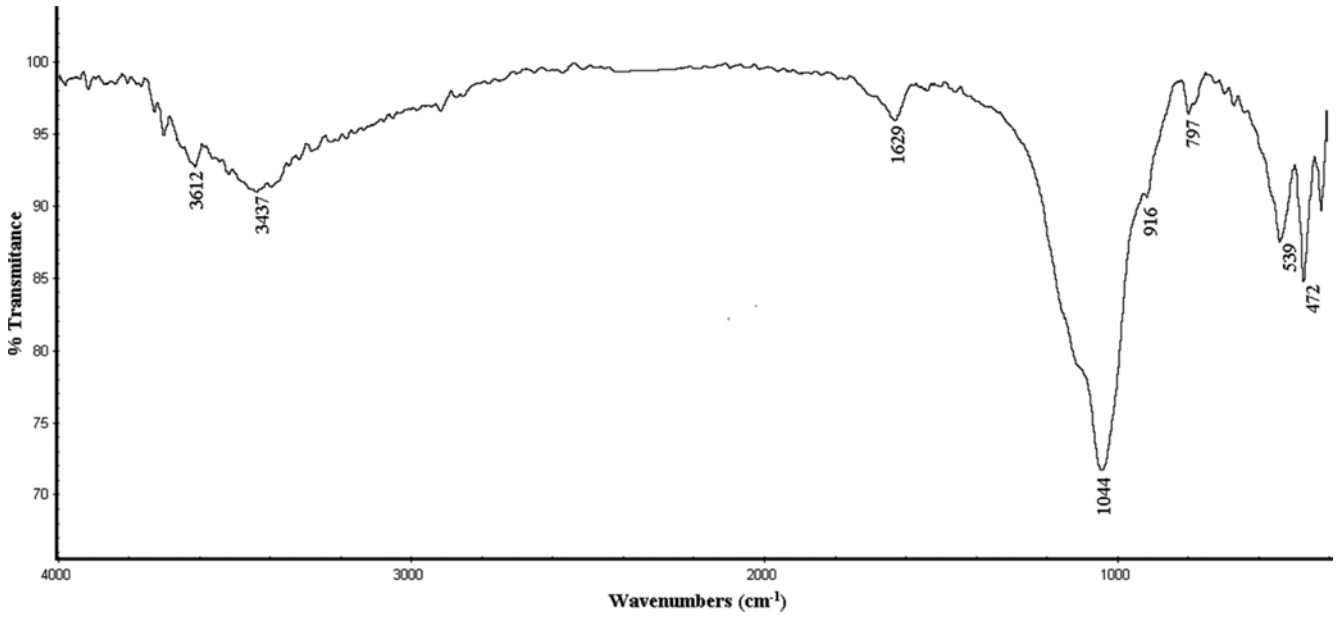

Fig. 1. FTIR spectrum of Al/nanoclay.

vibrations [20]. The bands at 3,437 cm^{-1} and 3,612 cm^{-1} correspond to H-O-H regarding adsorbed water for water present at the interlayer and Al-OH bond stretching, respectively. The band at 1,629 cm^{-1} was attributed to O-H bending, which confirmed the presence of hydration water [32]. The peaks at 472 and 539 cm^{-1} were attributed to Si-O-Si and Si-O-Al stretching vibrations, respectively.

The EDX elemental mapping images of Al, Si, O, Mg, Na, Fe, K, Ca, and S for AL/nanoclay can be seen in Fig. 2. The elemental analysis maps reveal the homogeneous distribution of all elements in the structure of nanoclay (Fig. 2). The weight percentages (wt%) of Al, Si, O, Fe, Na, Mg, Ca, and K elements within the nanoclay were 10.44, 32.78, 47.08, 5.53, 0.79, 1.32, 1.56 and 0.5%, respec-

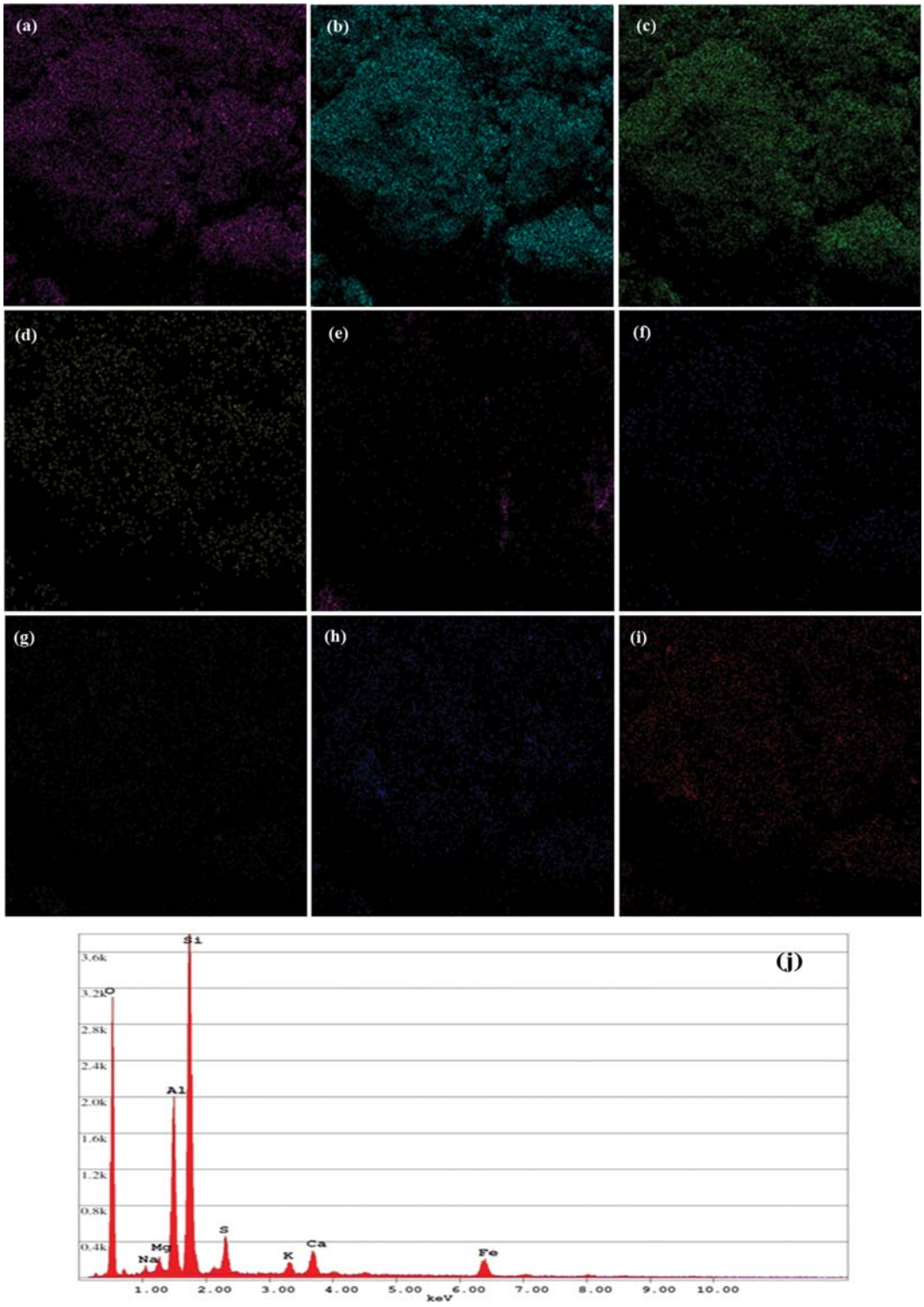

Fig. 2. Elemental analysis maps for (a) Al, (b) Si, (c) O, (d) Mg, (e) Na, (f) Fe, (g) K, (h) Ca, (i) S, and (j) the EDX spectrum of modified nanoclay.

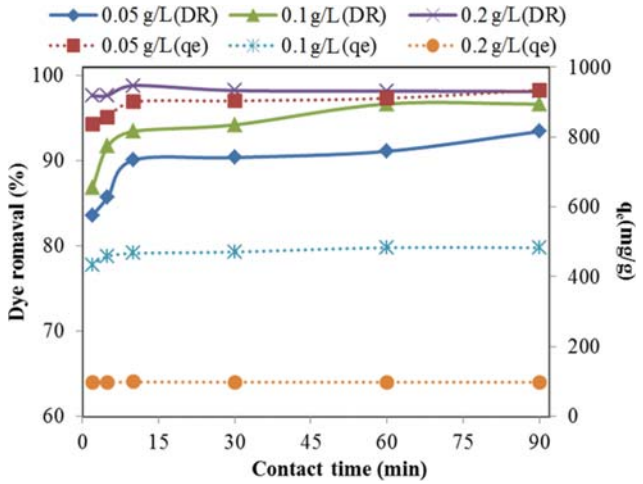

Fig. 3. Effect of contact time on the percent removal of DR23 (DR23 concentration: 50 mg/L, pH: 2, temperature: 25 °C).

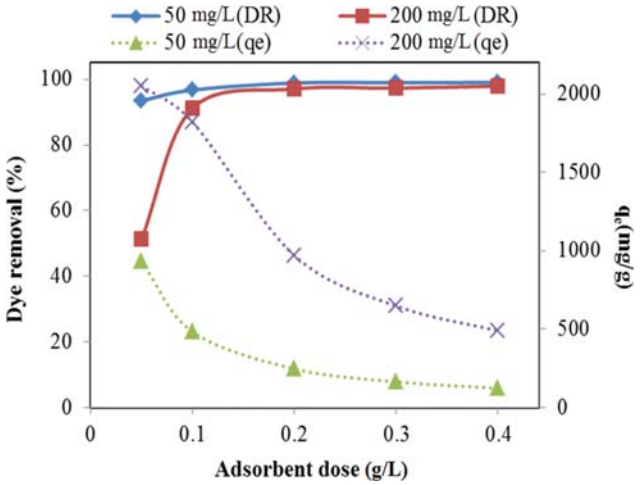

Fig. 4. Effect of adsorbent dose on the removal of DR23 (DR23 concentration: 50 and 200 mg/L, pH: 2, temperature: 25 °C).

tively [33]. Based on Fig. 2(j), the weight percentages (wt%) of Al, Si, O, Fe, Na, Mg, Ca, K, and S compounds within the Al/nanoclay were 12.9, 29.27, 45.38, 5.22, 0.61, 1.1, 1.37, 0.42 and 3.73%, respectively. The results show that the principal elements of Al/nanoclay were O, Si, and Al. In comparison to the nanoclay, the percentage content of Al in modified nanoclay was higher than raw nanoclay and the percentage content of Si, O, Fe, Na, Mg, Ca and K in the Al/nanoclay structure was lower. This may be due to the exchange of Al^{3+} ions with Na and Ca in the nanoclay structure. The result of FTIR and EDX reflected that the aluminum covering on the surface of nanoclay was successfully achieved.

2. The Effect of Contact Time on Dye Removal

The effect of contact time on the rate of sorption of DR23 by Al/nanoclay was investigated at different adsorbent doses (0.05, 0.1, and 0.2 g/L) and at time intervals ranging from 2 to 90 min. Fig. 3 shows the dye removal efficiency and the adsorption capacity as a function of contact time. As can be seen from Fig. 3, the adsorption rate was rapid in the initial stages of the adsorption process but before reaching the equilibrium it became slower. In addition, with increasing contact time, the adsorption capacity increased to a certain level and then remained almost constant. This may have been due to the large number of vacant surface sites which were available on the Al/nanoclay adsorbent at the preliminary stage of adsorption, but later the vacant sites were occupied by dye molecules which could create a repulsive force between the solute molecules on the adsorbent surface and bulk phase, so the dye adsorption by the remaining vacant sites was difficult [34]. A similar trend was observed for DR23 dye adsorption on biochar [35].

3. The Effect of Adsorbent Dose

The influence of adsorbent dose on DR23 adsorption was examined at two different initial dye concentrations of 50 and 200 mg/L. The Al/nanoclay doses varied from 0.05 to 0.4 g/L. It can be seen from Fig. 4 that the removal efficiency of DR23 dye increased sharply at a concentration of 200 mg/L with an increase in the adsorbent dose from 0.05 to 0.2 g/L. At 50 mg/L concentration, the percentage of dye removal increased at a slower rate. These results may be due to the availability of larger amounts of dye per unit of adsorbent at higher initial dye concentrations [36]. However, at a higher dose of 0.2 g/L, the adsorption efficiency was almost constant. This is probably because, as the Al/nanoclay adsorbent dose increased, a greater number of active sites and greater surface area were available; thus the adsorption rate was higher. But at higher doses, no significant changes in dye adsorption were observed, which is probably attributed to overlapping or accumulation of adsorption sites [37]. According to Fig. 4, the adsorption capacity decreased with the increase in Al/nanoclay dose. At low adsorbent dose, the active sites on the adsorbent surface were fully accessible for dye molecules, resulting in having higher adsorption capacity. But at higher adsorbent doses, most of the adsorption sites with low energy were first taken up by dye molecules. As a result, the number of available high-energy adsorption sites decreased, which reduced the adsorption capacity [38]. The result was in agreement with the previous study on dye adsorption [39].

4. The Effect of Initial Dye Concentration

Adsorption experiments with an initial dye concentration of 25-

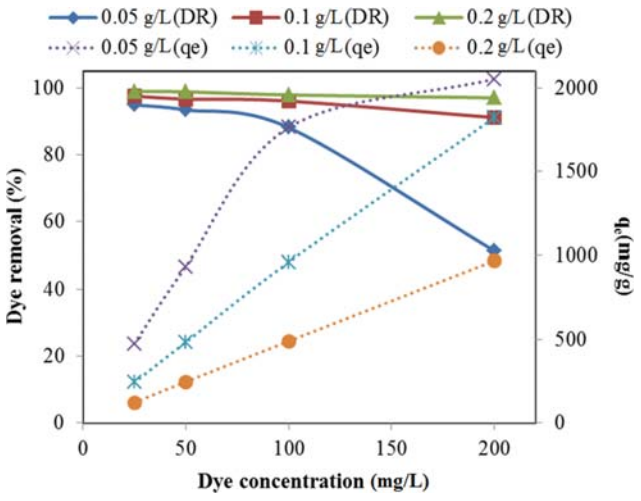

Fig. 5. Effect of initial dye concentration on the removal of DR23 (pH: 2, temperature: 25 °C).

200 mg/L were performed by different doses of the adsorbent. The effect of the initial DR23 concentration on the dye removal and adsorption capacity of the Al/nanoclay is illustrated in Fig. 5. As shown, the removal and adsorption capacity of the DR23 was different. As the initial dye concentration increased, the adsorption capacity increased while the dye removal efficiency decreased. This phenomenon is related to the number of active sites on the Al/nanoclay surface and the availability of DR23 molecules occupying the active sites. The higher dye adsorption efficiency at lower concentrations was due to the lower ratio of dye molecules in solution to the active sites and consequently, more adsorption sites were available, so the percentage of dye removal increased. The rate of dye adsorption decreased with increasing initial dye concentration, which may have been due to the adsorption sites being occupied by dye molecules and the sufficient number of active sites required for dye adsorption was reduced [40,41]. The results also show that at high concentrations of dye the adsorption capacity was high. It seems that increasing the concentration of the adsorbate leads to an increase in the driving force, which increases the amount of dye diffusion [42]. Similar observations have also been reported by other researchers [16,26].

5. The Effect of pH

The dye adsorption process is greatly affected by the solution pH due to its impact on the surface binding sites of adsorbent and ionization of the dye molecules [43]. The quantity of DR23 adsorption on Al/nanoclay at different pH values from 2 to 10 was studied for various doses of adsorbent using an initial dye concentration of 50 mg/L, as illustrated in Fig. 6. The maximum adsorption of DR23 was achieved at pH 2. The adsorption capacity and dye removal efficiency were significantly reduced by increasing the pH of the solution from 2 to 10. That is because, at low pH, the presence of hydrogen ions (H^+) can improve the positive charge of the Al/nanoclay surface; as a result, the adsorption capacity and efficiency of the DR23 anionic dye increased [44,45].

These results suggest that the dominant mechanism of DR23 dye adsorption by Al/nanoclay may be electrostatic attraction. The zeta potential can, to some extent, confirm the adsorption mechanism. The zeta potential of Al/nanoclay at a pH of 2 was +21 mV, while the zeta potential of DR23 was −23 mV. The positive zeta potential of Al/nanoclay might have been related to the Al^{3+} covered on the adsorbent. The negative zeta potential of DR23 was due to the presence of two sulfonic groups in its structure. DR23 dye in aqueous environment dissociated to the sulfonate anions ($R\text{-}SO_3^-$) and the sodium ions (Na^+). Although sulfonic groups at acidic pH can be protonated to the neutral form ($R\text{-}SO_3H$), but because the pKa values of sulfonic groups are below zero even in acidic solutions, they maintain their negative charge [46]. Hence, the results obtained by zeta potential confirm that the adsorbent surface is suitable for the adsorption of negative dye molecules, and strong electrostatic interaction is formed between the adsorbent and anionic adsorbate.

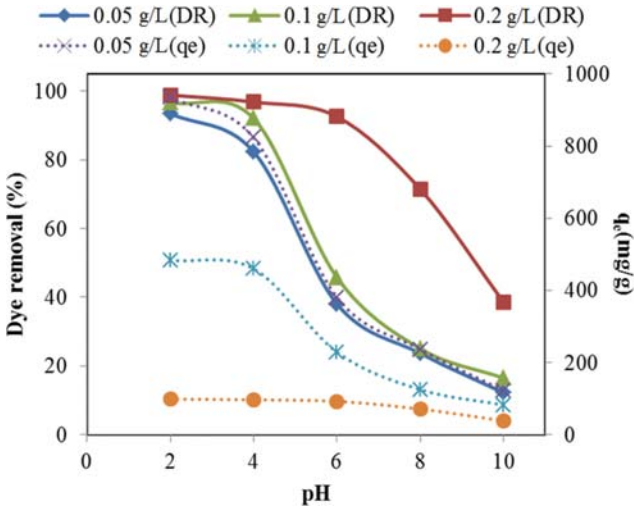

Fig. 6. Effect of pH on the removal of DR23 (DR23 concentration: 50 mg/L, temperature: 25 °C).

Besides, at low pH values, the aluminol groups on the surface of Al/nanoclay are protonated to the cationic form $AlOH^{2+}$, which enhances the adsorption of the negatively charged dye through

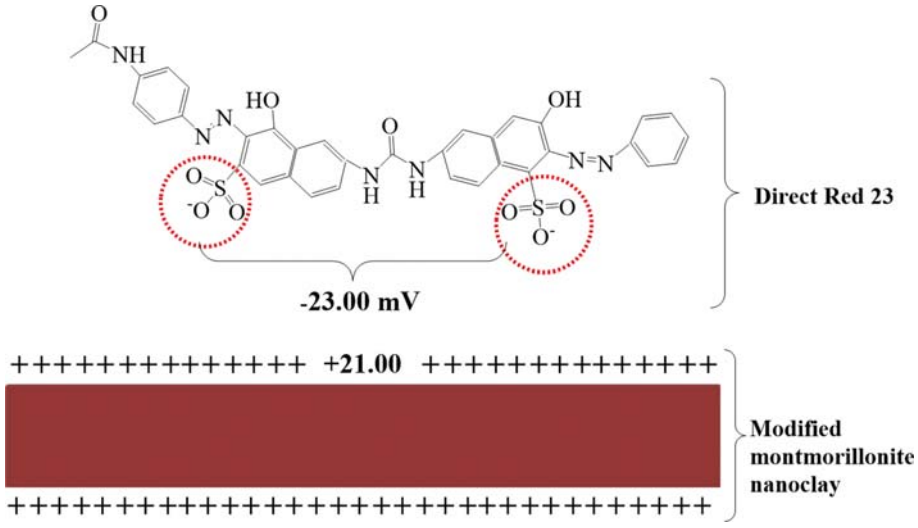

Fig. 7. Schematic mechanism of DR23 dye adsorption on the adsorbent.

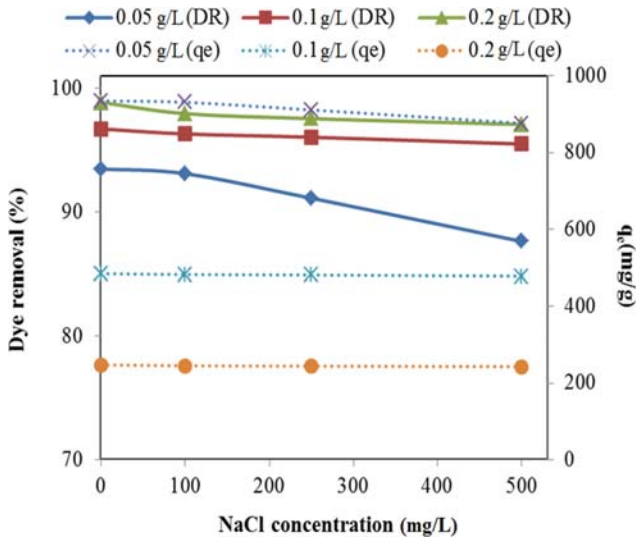

Fig. 8. Effect of ionic strength on the removal of DR23 (DR23 concentration: 50 mg/L, pH: 2, temperature: 25 °C).

electrostatic attraction. The mechanism of DR23 dye adsorption by Al/nanoclay is presented in Fig. 7. Similar findings have been reported for the DR23 dye adsorption onto graphene oxide [46] and corn stalk [47].

6. Effect of Ionic Strength on DR23 Dye Adsorption

Some ionic species which naturally exist in water can disrupt the adsorption process by competing with pollutants for binding to active sites [48]. The effect of ionic strength on uptake of DR23 dye was investigated by adding different NaCl concentrations ranging from 0 to 500 mg/L at different doses of Al/nanoclay. As is clear from Fig. 8, the amount of DR23 removal by Al/nanoclay was decreased with increasing concentration of NaCl in solution. The decline of the adsorption rate may be ascribed to the competition between chloride ions and the sulfonate groups of dye molecules for active sites of the Al/nanoclay surface [49]. Thus, the adsorption efficiency decreases by increasing ionic strength. However, the effect of the NaCl concentration on the adsorption capacity was not remarkable, and the high adsorption capacity of Al/nanoclay was maintained even at high salt concentration. Increasing ionic strength would be undesirable to the adsorption of anionic dye, as had previously been observed [50,51].

7. Kinetic Study

Kinetic studies are essential to obtain information about the mechanisms and rate-controlling steps of adsorption [52]. Pseudo-first-order, pseudo-second-order [53], and intra-particle diffusion [54] models were used to analyze the adsorption kinetic of the DR23 dye (Fig. 9). The equations on the kinetic models are given

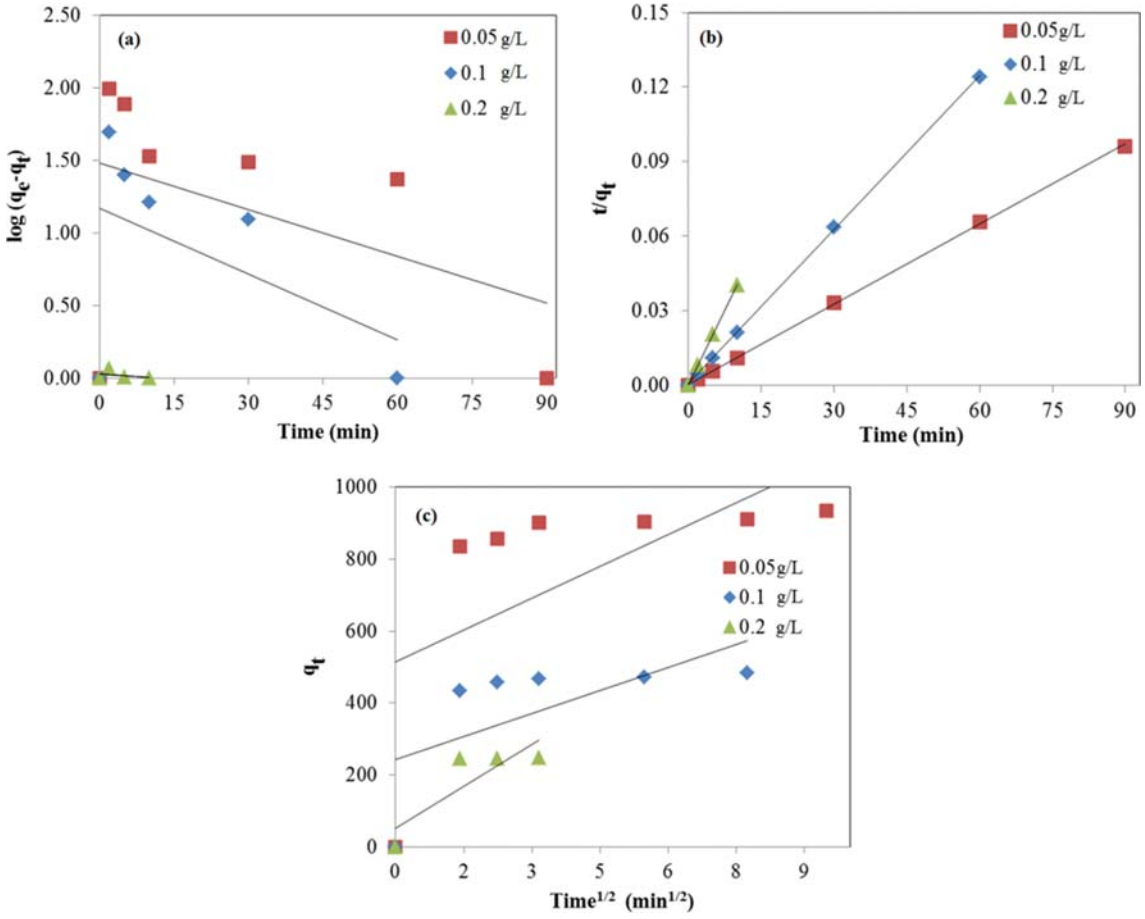

Fig. 9. (a) Pseudo-first-order, (b) pseudo-second-order, and (c) intra-particle diffusion kinetics for the adsorption of DR23 onto Al/nanoclay.

Table 1. Kinetic parameters for DR23 adsorption onto the Al/nanoclay

Kinetic model	Linear form of equation	Kinetic coefficient	Adsorbent dose (g/L)		
			0.05	0.1	0.2
Pseudo-first-order	$\log(q_e - q_t) = \log q_e - \frac{k_1 t}{2.303}$	k_1 (1/min)	0.024	0.034	0.005
		q_e (mg/g)	4.4	3.2	1.02
		R^2	0.197	0.23	0.118
Pseudo-second-order	$\frac{t}{q_t} = \frac{1}{k_2 q_e^2} + \frac{t}{q_e}$	k_2 (g/mg min)	0.003	0.007	0.177
		$q_{e,\,calculated}$ (mg/g)	909	476.2	250
		h	2,500	1,666	1,1111
		R^2	0.999	0.999	0.999
Intra-particle diffusion	$q_t = k_{id} t^{1/2} + C$	k_{id} (mg/g $min^{1/2}$)	59.11	42.73	77.86
		C (mg/g)	514.2	243.1	51.26
		R^2	0.368	0.4	0.725

in Table 1.

Where, q_t the amount of DR23 adsorbed (mg/g) at time t (min), k_1 is the pseudo-first-order adsorption rate coefficient (1/min) calculated from the slope of linear plot log ($q_e - q_t$) versus the time. k_2 is the rate constant of pseudo-second-order adsorption (g/mg min) calculated from the slope of the linear plot of t/q_t versus t [55]. k_{id} (mg/g $min^{1/2}$) is the intra-particle diffusion rate constant calculated from the slope of the linear plot of q_t versus $t^{1/2}$ [56], and C (mg/g) is related to the thickness of boundary layer. The higher C value in lower adsorbent dose indicates a larger boundary layer effect.

The plots for the pseudo-first-order, pseudo-second-order model, and intra-particle diffusion models are shown in Fig. 9, respectively. The calculated parameters of these kinetics models for DR23 adsorption are listed in Table 1. Since the plot of q_t versus $t^{1/2}$ does not provide a straight line, the adsorption process does not follow the intra-particle diffusion model. The calculated correlation coefficient (R^2) of the three models shows that the pseudo-second-order model was more suitable in DR23 adsorption process for all adsorbent doses. This is because of the higher correlation coefficient (R^2>0.999) of the pseudo-second-order model than the two other kinetics models. In addition, the rate coefficient of pseudo-second-order (k_2) increased by increasing adsorbent dose, which indicated the adsorption process was faster at higher doses of Al/nanoclay because there were more active sites on the adsorbent surface.

8. Isotherm Study

The Langmuir, Freundlich, and Dubinin-Radushkevich isotherms models have been used to describe the interaction behavior and to estimate the maximum adsorption capacity of Al/nanoclay for DR23 dye adsorption. The Langmuir isotherm describes the monolayer adsorption of pollutants onto the homogeneous adsorption sites on the solid surface where all the adsorptive sites are energetically equivalent [57]. Freundlich isotherm model can be applied to describe multilayer sorption at the heterogeneous adsorbent surface where each adsorptive site has specific bond energy [58]. Dubinin-Radushkevich (D-R) isotherm is used to describe the adsorption mechanism with a Gaussian energy distribution on the heterogeneous surfaces [34,59].

The linearized form of the isotherm models is represented in Table 2, where C_e (mg/L) is equilibrium DR23 dye concentration, q_e (mg/g) is the adsorption capacity at equilibrium condition, q_m (mg/g) represents the maximum adsorption capacity and b (L/mg) is the constant Langmuir related to the free energy of adsorp-

Table 2. Isotherm parameters for DR23 adsorption onto the Al/nanoclay

Adsorption isotherm	Linear form of equation	Isotherm coefficient	Adsorbent dose (g/L)		
			0.05	0.1	0.2
Langmuir	$\frac{1}{q_e} = \frac{1}{q_{max}} + \frac{1}{b q_{max}} \frac{1}{C_e}$	q_{max} (mg/g)	2,500	2,000	1,111
		b (L/mg)	0.19	0.227	0.5
		R^2	0.998	0.992	0.996
Freundlich	$\log q_e = \log k_f + \frac{1}{n} \log C_e$	K_F (mg/g)(L/mg)$^{1/n}$	567.9	356.2	318.1
		n	7.11	1.66	1.57
		R^2	0.83	0.98	0.99
Dubinin-Radushkevich	$\ln q_e = \ln q_m - \beta \varepsilon^2$	β (mol^2/J^2)	6×10^{-7}	3×10^{-7}	1×10^{-7}
		q_m (mg/g)	1,696.8	1,160.6	675.6
	$E = \frac{1}{(2\beta)^{1/2}}$	E (kJ/mol)	0.91	1.29	2.23
		R^2	0.89	0.79	0.87

tion. K_F (mg/g)(L/mg)$^{1/n}$ is the Freundlich constant, and n is the heterogeneity factor denoting the adsorption intensity [60]. β (mol^2/J^2) is D-R isotherm constant and E (kJ/mol) is the free energy of adsorption [61].

Fig. 10 shows the plots of Langmuir, Freundlich, and Dubinin-Radushkevich isotherms. The analysis of the isotherm data is represented in Table 2. According to the results, the Langmuir model was the best fit for the adsorption process because its correlation coefficient (R^2) was higher than other isotherm models. Favorable adsorption is illustrated by a value of n in the range between 1 and 10. Furthermore, 1/n being close to zero indicates a higher heterogeneity of the adsorbent surface [62]. The higher n value (lower 1/n) reflects the presence of high energy sites on the adsorbent surface and stronger adsorbent adsorbate interaction. Also, 1/n values

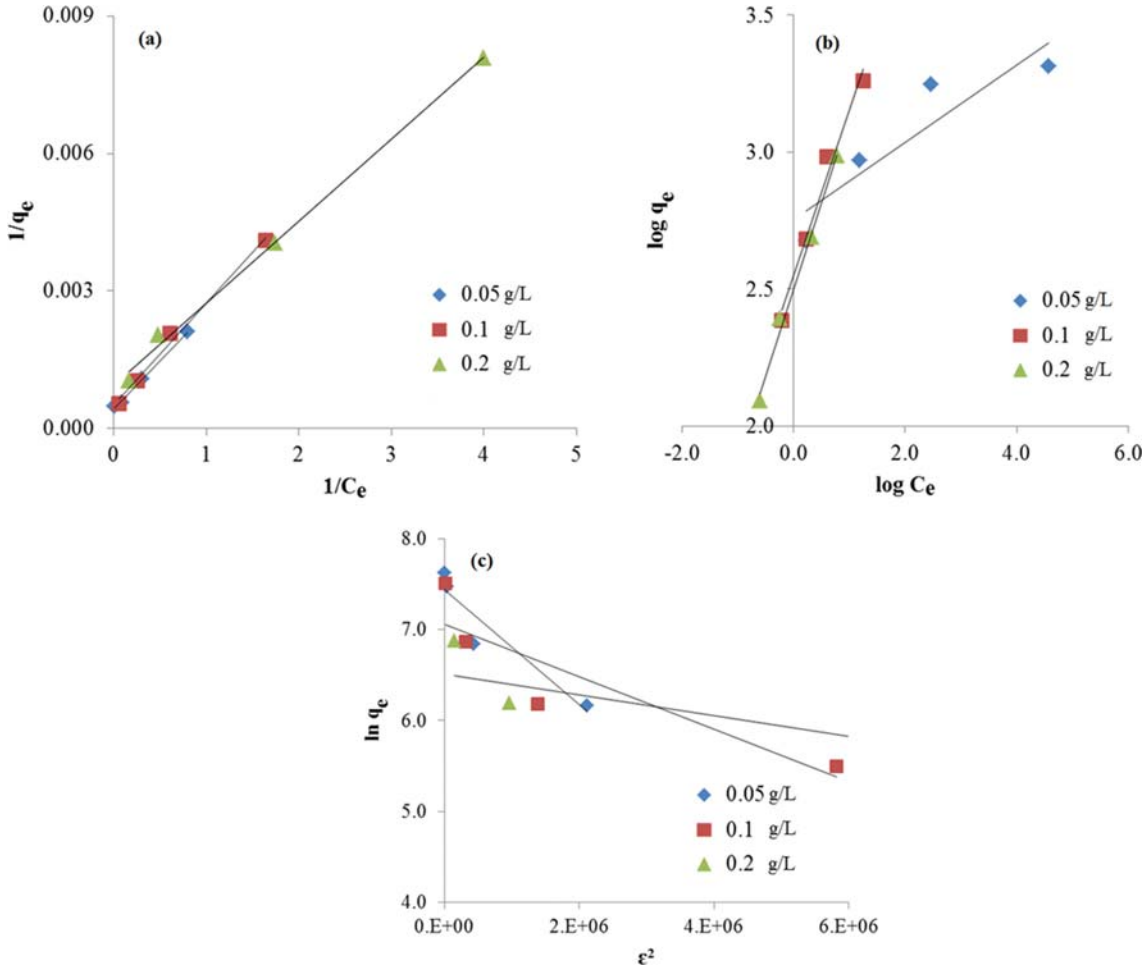

Fig. 10. (a) Langmuir, (b) Freundlich, and (c) Dubinin-Radushkevich isotherms for the adsorption of DR23 onto the Al/nanoclay.

Table 3. Comparison of adsorption capacity of some modified montmorillonite clays as adsorbent

Modified nanoclay	Dye	q_m (mg/g)	Source
Montmorillonite/cationic surfactants	Reactive Red 120	183	[66]
Montmorillonite/graphene oxide	Crystal violet	746.2	[67]
Montmorillonite/octadecylamine	Orange G	39.4	[27]
Montmorillonite/gemini surfactants	Methyl orange	16.1-271.7	[68]
Montmorillonite/supported porous carbon	Methyl blue	686.9	[69]
Novel kappacarrageenan/poly (vinyl alcohol) nanocomposite hydrogels	Crystal violet	151	[70]
Montmorillonite filled composite	Congo red	110	[71]
Starch montmorillonite/polyaniline	Reactive dye	91.7	[72]
Dodecyl sulfobetaine surfactant modified montmorillonite	Methylene blue	150.2	[73]
Lignocelluloseg-poly(acrylic acid)/montmorill onite hydrogel nanocomposites	Methylene blue	1,994.3	[74]
Al/nanoclay	Direct Red 23	2,500	This study

were close to 0, suggesting heterogeneous surface of Al/nanoclay [63].

The maximum monolayer adsorption capacity of Al/nanoclay for DR23 was found to be 2,500 mg/g, and it is much higher than the pure nanoclay (166.6 mg/g), which was studied in the previous study [33]. The maximum DR23 dye adsorption capacity by other adsorbents, such as corn stalk [47], powdered tourmaline [46], magnetic multi-walled carbon nanotubes-Fe3C [64] and CTAB-functionalized aqai stalk [65] was 51.87 mg/g, 153 mg/g, 172.4 mg/g, and 454.9 mg/g, respectively. In addition, Table 3 shows the comparison of the Al/nanoclay adsorption capacity with other modified montmorillonite for different types of dyes. From the results given in Table 3, it is evident that this novel superadsorbent, in comparison to other modified clays, is more efficient in dye removal; thus it can be used as an adsorbent for the purification of colored wastewater.

CONCLUSION

The application of alum modified montmorillonite nanoclay was considered for the adsorption of DR23 dye from aqueous solution. EDX and FTIR analysis confirmed that Al/nanoclay was successfully synthesized. The data showed that by increasing contact time and adsorbent dose and decreasing pH, initial dye concentration, and ionic strength, dye removal efficiency increases. In addition, pH has a significant effect on the adsorption process and the highest percentage of DR23 dye removal (98.8%) was obtained at pH 2. Zeta potential measurement showed that the zeta potential of Al/nanoclay was +21 mV, while the zeta potential of DR23 was −23 mV. This result indicates that high-efficiency removal of DR23 is attributed to the electrostatic interaction between the adsorbent and the anionic dye. The pseudo-second-order kinetic model and the Langmuir isotherm were found to best describe the DR23 adsorption, and the maximum monolayer adsorption capacity was 2,500 mg/g. The findings indicated that Al/nanoclay could be considered as an effective super adsorbent for the treatment of colored wastewater.

ACKNOWLEDGEMENT

This study was financially supported by Shahid Sadoughi University of Medical Sciences (Grant no: 7903).

REFERENCES

1. N. M. Mahmoodi, J. Abdi, M. Oveisi, M. A. Asli and M. Vossoughi, *Mater. Res. Bull.*, **100**, 357 (2018).
2. S. A. Khan, S. B. Khan, A. Farooq and A. M. Asiri, *Int. J. Biol. Macromol.*, **130**, 288 (2019).
3. N. Liu, H. Wang, C. H. Weng and C. C. Hwang, *Arabian J. Chem.*, **11**, 1281 (2018).
4. M. Ismail, M. Khan, S. B. Khan, K. Akhtar, M. A. Khan and A. M. Asiri, *J. Mol. Liq.*, **268**, 87 (2018).
5. A. C. Lucilha, C. E. Bonancêa, W. J. Barreto and K. Takashima, *Spectrochim. Acta, Part A*, **75**, 389 (2010).
6. A. Paz, J. Carballo, M. J. Pérez and J. M. Domínguez, *Chemosphere*, **181**, 168 (2017).
7. C. S. Rodrigues, L. M. Madeira and R. A. Boaventura, *Environ. Technol.*, **34**, 719 (2013).
8. M. Y. A. Mollah, J. A. Gomes, K. K. Das and D. L. Cocke, *J. Hazard. Mater.*, **174**, 851 (2010).
9. Y. Pan, Y. Wang, A. Zhou, A. Wang, Z. Wu, L. Lv, X. Li, K. Zhang and T. Zhu, *Chem. Eng. J.*, **326**, 454 (2017).
10. N. C. Dias, J. P. Bassin, G. L. Sant'Anna Jr. and M. Dezotti, *Int. Biodeter. Biodegr.*, **144**, 104742 (2019).
11. S. H. S. Chan, T. Y. Wu, J. C. Juan and C. Y. Teh, *J. Chem. Technol. Biotechnol.*, **86**, 1130 (2011).
12. S. M. Pormazar and A. Dalvand, *Int. J. Environ. Anal. Chem.*, **1** (2020).
13. M. S. Nawaz and M. Ahsan, *Alex. Eng. J.*, **53**, 717 (2014).
14. G. K. Cheruiyot, W. C. Wanyonyi, J. J. Kiplimo and E. N. Maina, *Sci. Afr.*, **5**, e00116 (2019).
15. R. Salehi, F. Dadashian and E. Ekrami, *Prog. Color Colorants Coat.*, **11**, 9 (2018).
16. S. Afshin, S. A. Mokhtari, M. Vosoughi, H. Sadeghi and Y. Rashtbari, *Data Brief.*, **21**, 1008 (2018).
17. E. Alver and A. Ü. Metin, *Chem. Eng. J.*, **200**, 59 (2012).
18. D. Sun, X. Zhang, Y. Wu and X. Liu, *J. Hazard. Mater.*, **181**, 335 (2010).
19. O. Acisli, A. Khataee, S. Karaca and M. Sheydaei, *Ultrason. Sonochem.*, **31**, 116 (2016).
20. D. A. Almasri, T. Rhadfi, M. A. Atieh, G. McKay and S. Ahzi, *Chem. Eng. J.*, **335**, 1 (2018).
21. J. Chang, J. Ma, Q. Ma, D. Zhang, N. Qiao, M. Hu and H. Ma, *Appl. Clay. Sci.*, **119**, 132 (2016).
22. R. Zhu, Q. Chen, Q. Zhou, Y. Xi, J. Zhu and H. He, *Appl. Clay. Sci.*, **123**, 239 (2016).
23. M. Ghadiri, W. Chrzanowski and R. Rohanizadeh, *RSC Adv.*, **5**, 29467 (2015).
24. P. Huang, A. Kazlauciunas, R. Menzel and L. Lin, *ACS Appl. Mater. Interfaces*, **9**, 26383 (2017).
25. Y. Liu, X. Cao, Z. Yu, X. Song and L. Qiu, *Marine. Pollution. Bull.*, **103**, 211 (2016).
26. A. Hassani, R. D. C. Soltani, M. Kıranşan, S. Karaca, C. Karaca and A. Khataee, *Korean J. Chem. Eng.*, **33**, 178 (2016).
27. M. A. Salam, S. A. Kosa and A. A. Al-Beladi, *J. Mol. Liq.*, **241**, 469 (2017).
28. A. Dalvand, E. Gholibegloo, M. R. Ganjali, N. Golchinpoor, M. Khazaei, H. Kamani, S. S. Hosseini and A. H. Mahvi, *Environ. Sci. Pollut. Res.*, **23**, 16396 (2016).
29. S. Pourshadlou, I. Mobasherpour, H. Majidian, E. Salahi, F. S. Bidabadi, C. T. Mei and M. Ebrahimi, *J. Colloid Interface Sci.*, **568**, 245 (2020).
30. N. M. Mahmoodi and M. H. Saffar-Dastgerdi, *Microchem. J.*, **145**, 74 (2019).
31. Z. Zhu, S. Ouyang, P. Li, L. Shan, R. Ma and P. Zhang, *Appl. Clay. Sci.*, **188**, 105500 (2020).
32. O. Ayodele, J. Lim and B. Hameed, *Appl. Catal., A*, **413**, 301 (2012).
33. A. H. Mahvi and A. Dalvand, *Water Qual. Res. J.*, **55**, 132 (2020).
34. S. Banerjee and M. C. Chattopadhyaya, *Arabian J. Chem.*, **10**, S1629 (2017).
35. N. Liu, M. Zhu, H. Wang and H. Ma, *J. Mol. Liq.*, **223**, 335 (2016).

36. H. Abbasi and H. Asgari, *Global Nest J.*, **20**, 582 (2018).
37. A. A. Inyinbor, F. A. Adekola and G. A. Olatunji, *Water Resour. Ind.*, **15**, 14 (2016).
38. Y. Li, H. Lu, Y. Wang, Y. Zhao and X. Li, *J. Mater. Sci.*, **54**, 7603 (2019).
39. F. A. Ngwabebhoh, M. Gazi and A. A. Oladipo, *Chem. Eng. Res. Des.*, **112**, 274 (2016).
40. R. Huang, Q. Liu, J. Huo and B. Yang, *Arabian J. Chem.*, **10**, 24 (2017).
41. M. A. M. Salleh, D. K. Mahmoud, W. A. W. A. Karim and A. Idris, *Desalination*, **280**, 1 (2011).
42. A. B. Albadarin, M. N. Collins, M. Naushad, S. Shirazian, G. Walker and C. Mangwandi, *Chem. Eng. J.*, **307**, 264 (2017).
43. I. Hussain, Y. Li, J. Qi, J. Li and L. Wang, *J. Environ. Manage.*, **215**, 123 (2018).
44. A. Kausar, M. Iqbal, A. Javed, K. Aftab, Z. I. H. Nazli, H. N. Bhatti and S. Nouren, *J. Mol. Liq.*, **256**, 395 (2018).
45. S. M. Pormazar, M. H. Ehrampoush, M. T. Ghaneian, M. Khoobi, P. Talebi and A. Dalvand, *Korean J. Chem. Eng.*, **37**, 93 (2020).
46. W. Konicki, M. Aleksandrzak, D. Moszyński and E. Mijowska, *J. Colloid Interface Sci.*, **496**, 188 (2017).
47. M. R. Fathi, A. Asfaram and A. Farhangi, *Spectrochim. Acta, Part A*, **135**, 364 (2015).
48. P. H. Chang, Z. Li, J. S. Jean, W. T. Jiang, C. J. Wang and K. H. Lin, *Appl. Clay. Sci.*, **67**, 158 (2012).
49. M. H. Kim, C. H. Hwang, S. B. Kang, S. Kim, S. W. Park, Y. S. Yun and S. W. Won, *Chem. Eng. J.*, **280**, 18 (2015).
50. L. Mouni, L. Belkhiri, J. C. Bollinger, A. Bouzaza, A. Assadi, A. Tirri, F. Dahmoune, K. Madani and H. Remini, *Appl. Clay. Sci.*, **153**, 38 (2018).
51. H. Y. Zhu, R. Jiang and L. Xiao, *Appl. Clay. Sci.*, **48**, 522 (2010).
52. R. A. Fideles, G. M. D. Ferreira, F. S. Teodoro, O. F. H. Adarme, L. H. M. da Silva, L. F. Gil and L. V. A. Gurgel, *J. Colloid Interface Sci.*, **515**, 172 (2018).
53. Z. Harrache, M. Abbas, T. Aksil and M. Trari, *Microchem. J.*, **144**, 180 (2019).
54. F. Deniz and S. Karaman, *Microchem. J.*, **99**, 296 (2011).
55. A. F. Hassan, A. M. Abdel-Mohsen and M. M. G. Fouda, *Carbohydr. Polym.*, **102**, 192 (2014).
56. M. Elhadj, A. Samira, T. Mohamed, F. Djawad, A. Asma and N. Djamel, *Sep. Sci. Technol.*, **55**, 867 (2020).
57. H. N. Bhatti, A. Jabeen, M. Iqbal, S. Noreen and Z. Naseem, *J. Mol. Liq.*, **237**, 322 (2017).
58. T. Maneerung, J. Liew, Y. Dai, S. Kawi, C. Chong and C. H. Wang, *Bioresour. Technol.*, **200**, 350 (2016).
59. H. S. Shin and J. H. Kim, *Process Biochem.*, **51**, 917 (2016).
60. C. Li, H. Xia, L. Zhang, J. Peng, S. Cheng, J. Shu and S. Zhang, *Res. Chem. Intermed.*, **44**, 2231 (2018).
61. G. Bayramoglu and M. Yilmaz, *Fiber Polym.*, **19**, 877 (2018).
62. N. H. Othman, N. H. Alias, M. Z. Shahruddin, N. F. A. Bakar, N. R. N. Him and W. J. Lau, *J. Environ. Chem. Eng.*, **6**, 2803 (2018).
63. D. N. R. de Sousa, S. Insa, A. A. Mozeto, M. Petrovic, T. F. Chaves and P. S. Fadini, *Chemosphere*, **205**, 137 (2018).
64. W. Konicki, I. Pełech, E. Mijowska and I. Jasińska, *Chem. Eng. J.*, **210**, 87 (2012).
65. F. M. Kasperiski, E. C. Lima, G. S. d. Reis, J. B. da Costa, G. L. Dotto, S. L. Dias, M. R. Cunha, F. A. Pavan and C. S. Correa, *Chem. Eng. Commun.*, **205**, 1520 (2018).
66. N. M. Mahmoodi, A. Taghizadeh, M. Taghizadeh and M. Azimi Shahali Baglou, *J. Environ. Chem. Eng.*, **7**, 103243 (2019).
67. C. Puri and G. Sumana, *Appl. Clay. Sci.*, **166**, 102 (2018).
68. Z. Luo, M. Gao, Y. Ye and S. Yang, *Appl. Surf. Sci.*, **324**, 807 (2015).
69. J. Yin, M. Pei, Y. He, Y. Du, W. Guo and L. Wang, *RSC Adv.*, **5**, 89839 (2015).
70. H. Hosseinzadeh, S. Zoroufi and G. R. Mahdavinia, *Polym. Bull.*, **72**, 1339 (2015).
71. R. Bhattacharyya and S. K. Ray, *Chem. Eng. J.*, **260**, 269 (2015).
72. A. Olad and F. F. Azhar, *Fiber Polym.*, **15**, 1321 (2014).
73. H. Fan, L. Zhou, X. Jiang, Q. Huang and W. Lang, *Appl. Clay. Sci.*, **95**, 150 (2014).
74. Y. Shi, Z. Xue, X. Wang, L. Wang and A. Wang, *Polym. Bull.*, **70**, 1163 (2013).